The Effect of Rotating Magnetic Fields on the Growth of SiGe Using the Traveling Solvent Method

T. J. Jaber[1] and M. Z. Saghir[1]

Abstract: The study deals with three-dimensional numerical simulations of fluid flow and heat transfer under the effect of a rotating magnetic field (RMF) during the growth of $Ge_{0.98}Si_{0.02}$ by the traveling solvent method (TSM). By using a RMF, an attempt is made to suppress buoyancy convection in the $Ge_{0.98}Si_{0.02}$ solution zone in order to get high quality and homogeneity with a flat growth interface. The full steady-state Navier-Stokes equations, as well as the energy, mass transport and continuity equations, are solved numerically using the finite element method. Different magnetic field intensities (B=2, 4, 10, 15 and 22 mT) for different rotational speeds (2, 7 and 10 rpm) under uniform and non-uniform heater profile conditions are considered. The results show that the RMF has a marked effect on the silicon concentration near the growth interface, changing the shape of the concentration profile from convex to nearly flat when the magnetic field intensity increases

keyword: Silicon (Si), Germanium (Ge), Traveling solvent method (TSM), Rotating magnetic field (RMF), Growth interface, Dissolution interface.

1 Introduction

Several techniques are currently used in industry for crystal growth such as the Bridgman method (Yu *et al,.*(2001), the Float Zone (Campbell *et al.,* 2001; Lappa, 2005, Gelfgat et al., 2005; Lan and Yeh, 2005), the Czochralski method (Tsukada *et al*., 2005), LPEE method, Liu *et al.* (2002), and Traveling solvent Method (TSM), Abidi *et al* (2005) and Okano *et al.* (2002). The TSM also known as the traveling Heater method (THM), is a very promising solution technique for growing high-quality bulk single crystals. It is based on a relatively new strategy to grow a single crystal without going through a high-temperature melt phase as in Float zone or in the Bridgman technique. By TSM, crystals can be grown at relatively low temperatures.

The TSM has been tested on many alloys producing uniform and uncontaminated crystal products. The ampoule in this technique contains the seed material at the bottom, a "solution" zone in the middle and the feed material at the top. The heated solution zone passes through the polycrystalline feed rod obtaining a single crystal by subsequent recrystallization. This solution zone is heated by radiation usually given by halogen lamps encompassed in a mirror furnace. Several related numerical studies have appeared in the literature over recent years.

Lent *et al*. (2002) conducted numerical simulations of $Ga_{1-x}In_xSb$ bulk single crystals. They realized that convective fluid flow, which is caused by gravity, plays an important role in this process. In order to suppress the undesired convective fluid flow in the solvent they applied different levels of magnetic induction (see also Ma and Walker, 2006). These authors also considered a small misalignment of the magnetic field and found that an increase in mixing in the horizontal plane is beneficial for the growth process.

More recently, Abidi *et al.* (2005) have carried out a three dimensional numerical simulation of the effect of an axial magnetic field during the growth of GeSi crystal by TSM. It has been shown that an external magnetic field makes the silicon distribution in the horizontal plane more homocentric and wider in the vertical plane.

CdTe and $CdTe_{0.9}Se_{0.9}$ crystals grown by the THM using a rotating magnetic field (RMF) were investigated by Salk *et al*. (1994). They showed that the rotating magnetic field generates a stable steady flow in the Te solution zone, improving the radial and axial distribution of the Te inclusions.

Liu *et al.* (2003) presented a 3D numerical simulation for the growth of CdTe single crystals under an applied axial static magnetic field. The effect of different magnetic field intensities on the flow, concentration distribution and the temperature fields in the solvent were examined. These authors illustrated that an external station-

[1] Department of Mechanical and Industrial Engineering, Ryerson University, 350 Victoria St., Toronto, ON, M5B 2K3

Polycrystalline $Ge_{1-x}Si_x$ Feed Rod

Dissolution interface

GeSi Melt

Growth interface

Ge Seed Crystal

Heater

Processed GeSi Crystal Growth

Heater

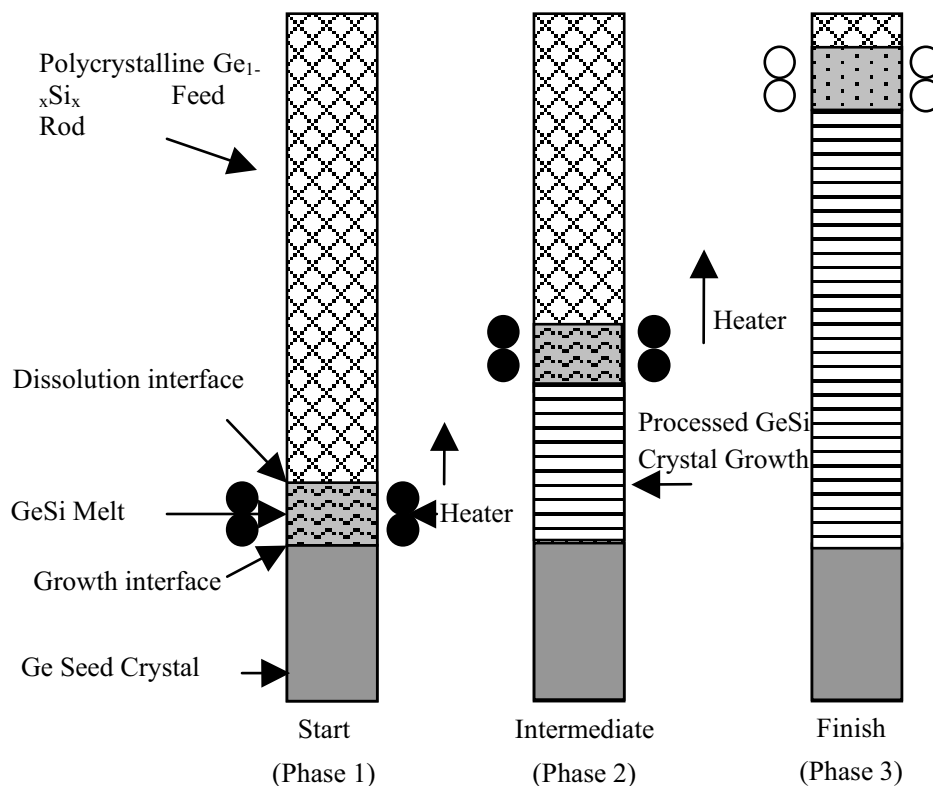Start (Phase 1)   Intermediate (Phase 2)   Finish (Phase 3)

Figure 1 : The traveling solvent method process

ary magnetic field is beneficial to suppress the convective fluid flow in the solvent.

Senchenkov *et al.* (1999) studied a single crystal growth of $Cd_xHg_{1-x}Te$ (x ≈ 0.2) by using the THM within a RMF of 2−−6 mT. It was found that an adequate choice of the magnetic induction value can lead to the required growing interface shape and to large diameter crystals with a radial crystal homogeneity that meets the requirements of the industry.

Liu *et al.* (2002) presented a continuum model for the liquid phase electroepitaxial (LPEE) growth process of GaAs semiconductor under a stationary magnetic field. For weak magnetic induction, a significant reduction in the flow intensity was observed, which is desirable for crystal growth. In addition, they observed the convective cells to be shifted to the vertical wall of the crucible with the consequent creation of a Hartmann layer. At higher magnetic induction the Hartman layer became thinner and the flow became homocentric and axisymmetric. It was found that the applied magnetic induction suppressed the flow in the growth system.

Okano *et al.* (2002) focused on controlling the interface shape. They examined how this crystal interface shape is affected by the crucible temperature, crucible rotation and crucible material. Their numerical model employed actual temperature profiles obtained from experimental process. It was reported that by increasing the temperature the interface curvature became larger. The application of rotation was successful in suppressing the natural convection in the solution, and an interface with less curvature for both the higher and lower temperature cases was achieved.

Figure 1 shows a schematic diagram of the TSM process considered in this study. The solution zone is heated by the heating elements and melt achieves a steady state (Phase1).

It is worth mentioning that the melting temperature of the $Ge_{0.98}Si_{0.02}$ material is less than the $Ge_{0.85}Si_{0.15}$ rod (Fig. 2).

Since silicon has a higher melting temperature than germanium, by having a higher concentration of silicon in the source we are able to keep the solvent in a liquid state while maintaining dissolution interface without any melting. This procedure allows the silicon from the Si-
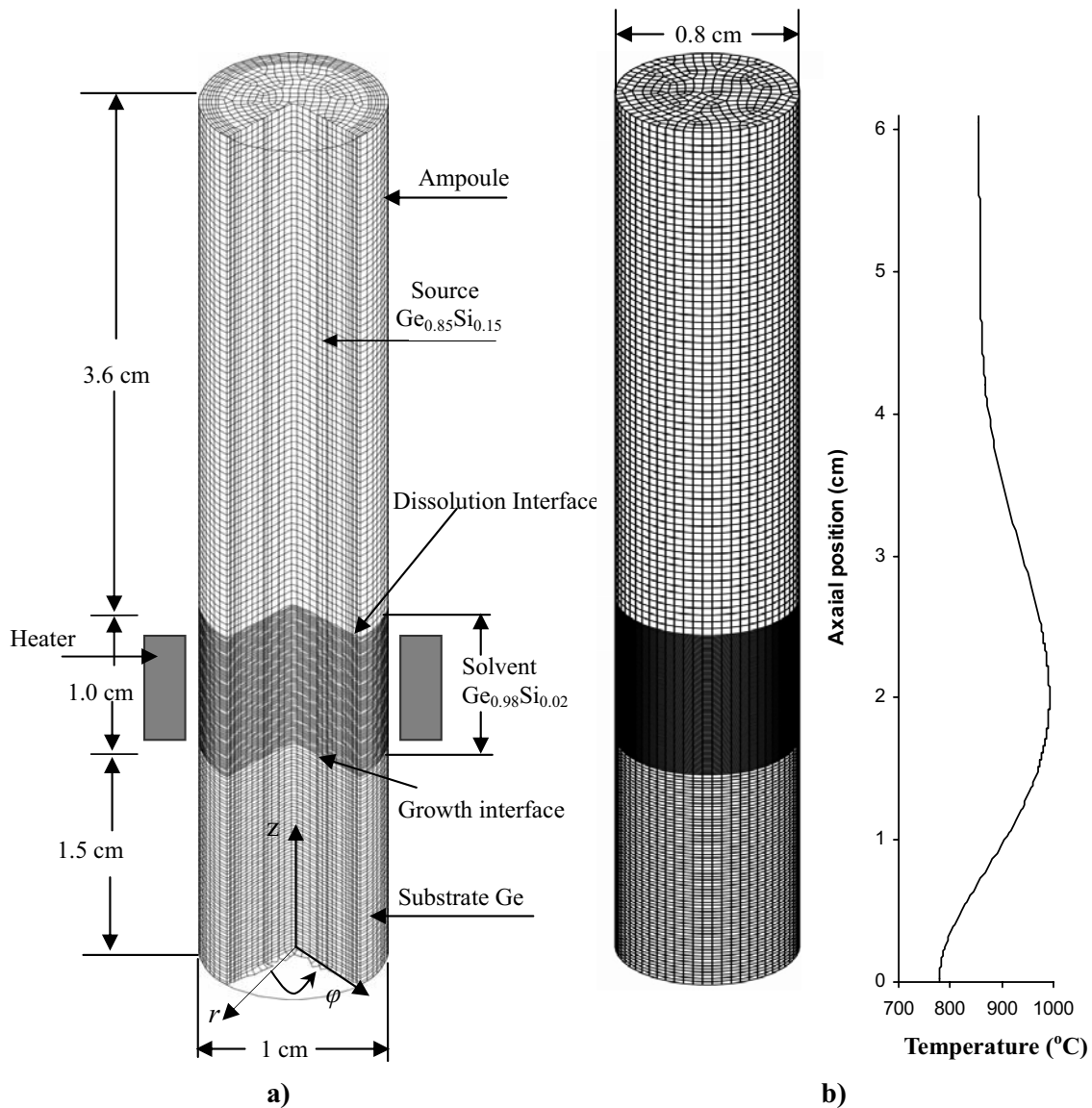
Figure 2 : Finite Element Model. **a)** Whole Model with ampoule **b)** Finite element mesh with experimentally measured heater thermal profile.

rich source to dissolve slowly through the solvent leading to the diffusion and transport of the silicon to the growth interface for crystallization.

The TSM ampoule is then translated downwards to the central axis of the furnace (Phase2). By downward movement of the ampoule more materials dissolve and at the same time crystallization takes place according to the lower temperature at the growth interface. The last phase, the heater is shut off and the molten region at the top of formed single crystal is allowed to cool and solidify ending the crystal process (Phase3).

The present study considers, in particular, the application of a rotating magnetic field. The full steady state Navier-Stokes equations, energy, continuity and mass transfer equations are solved numerically using the finite element technique. Section two presents the model description; section three explains in details the differential equation used to solve the problem. The solution technique is explained in section 4 and the results and discussions are shown in section 5.

The present study can be regarded as an extension of the earlier work of Sohail and Saghir (2006).
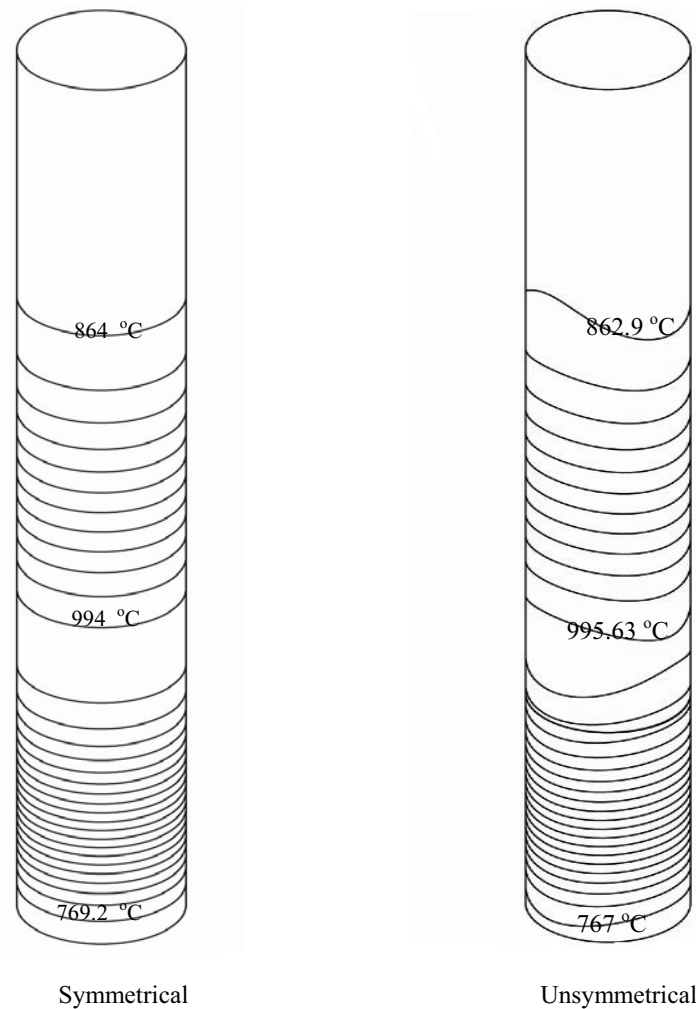
Symmetrical   Unsymmetrical

Figure 3 : Temperature heater thermal profile applied to the TSM Model.

2   Model Description

The schematic diagram for this study is illustrated in Figure 2. The model is described by a fixed cylindrical coordinate system (r, ϕ, z) that has the origin at the center base of the model. The model is 6.1 cm long and has a diameter 0.8 cm. It consists of a $Ge_{0.85}Si_{0.15}$ source rod (feedrod) having a length of 3.6 cm. This rod is located on top of a $Ge_{0.98}Si_{0.02}$ solvent zone having the same diameter and a length of 1.0 cm. At the bottom is the germanium seed (substrate) having a length of 1.5 cm and it also has the same diameter. The total sample is enclosed in an ampoule (quartz tube) having a wall thickness of 0.1 cm. The temperature profile measured experimentally at Dalhousie University is applied at the external surface of the quartz tube, see Figure 2b. Two different heater profiles were applied to this model, one having symmetric uniform heating around the sample, and the other having an unsymmetrical non-uniform heating, see Figure 3. The electromagnetic stirring of the solution is achieved by a rotating magnetic field of intensity and angular frequency (ω) placed around the heater ring.

3   Governing Equations

3.1   Navier-Stokes Equations

The motion of a laminar Newtonian fluid is governed by the Navier-Stokes equations:

r - component

$$\rho \left[u\frac{\partial u}{\partial r} + \frac{v}{r}\frac{\partial u}{\partial \varphi} + w\frac{\partial u}{\partial z} - \frac{v^2}{r} \right] = -\frac{\partial p}{\partial r}$$

$$+ \mu \left[\nabla^2 u - \frac{u}{r^2} - \frac{2}{r^2}\frac{\partial v}{\partial \varphi} \right] + F_r^M \qquad (1)$$

ϕ - component

$$\rho \left[u\frac{\partial v}{\partial r} + \frac{v}{r}\frac{\partial v}{\partial \phi} + w\frac{\partial v}{\partial z} + \frac{vu}{r} \right] = -\frac{1}{r}\frac{\partial p}{\partial \phi}$$

$$+ \mu \left[\nabla^2 v - \frac{v}{r^2} + \frac{2}{r^2}\frac{\partial v}{\partial \phi} \right] + F_\phi^M \qquad (2)$$

z- component

$$\rho \left[u\frac{\partial w}{\partial r} + \frac{v}{r}\frac{\partial w}{\partial \phi} + w\frac{\partial w}{\partial z} \right] = -\frac{\partial p}{\partial z}$$

$$+ \mu \left[\nabla^2 w \right] + F_z^M + g\rho \left[\beta_T (T - T_o) - \beta_c (c - c_o) \right] \qquad (3)$$

Where the Laplacian operator is given by

$$\nabla^2 = \left(\frac{1}{r}\frac{\partial}{\partial r}\left(r\frac{\partial}{\partial r} \right) + \frac{1}{r^2}\frac{\partial^2}{\partial \phi^2} + \frac{\partial^2}{\partial z^2} \right) \qquad (4)$$

Equation (1) to equation (3) correspond to the momentum equations in the solvent region in the radial (r), angular (ϕ) and axial (z) directions. In these equations u and v and w are the three velocity components in the radial (r), angular (ϕ) and axial (z) directions, and v, p, T, T_o, c, c_o, ρ, β_T, and β_c are the kinematic viscosity, pressure, temperature, melt temperature (also used as the reference temperature), silicon concentration, reference silicon concentration, solution density, thermal and solutal volume expansion coefficients, respectively. The three forces F_r^M, F_z^M and F_ϕ^M denote the magnetic body force components along r, z ϕ–directions, respectively.

3.2 Energy Equation

The energy equation in the solvent region can be represented as follows:

$$\rho c_p \left[u\frac{\partial T}{\partial r} + \frac{v}{r}\frac{\partial T}{\partial \phi} + w\frac{\partial T}{\partial z} \right]$$

$$= k \left(\frac{1}{r}\frac{\partial}{\partial r}\left(r\frac{\partial T}{\partial r} \right) + \frac{1}{r^2}\frac{\partial^2 T}{\partial \phi^2} + \frac{\partial^2 T}{\partial z^2} \right) \qquad (5)$$

Where k and c_p denote the thermal conductivity and the specific heat of the solvent. In the solid phases the energy equation reads:

$$\frac{\kappa_s}{\rho_s c_{p,s}} \left(\frac{1}{r}\frac{\partial}{\partial r}\left(r\frac{\partial T}{\partial r} \right) + \frac{1}{r^2}\frac{\partial^2 T}{\partial \phi^2} + \frac{\partial^2 T}{\partial z^2} \right) = 0 \qquad (6)$$

Where ρ_s, κ_s and $c_{p,s}$ denote the density, thermal conductivity, and specific heat of solid phases, respectively, Saghir (1987).

3.3 Continuity equation

$$\frac{1}{r}\frac{\partial}{\partial r}(ru) + \frac{1}{r}\frac{\partial v}{\partial \phi} + \frac{\partial w}{\partial z} = 0 \qquad (7)$$

3.4 Solute equation

The mass transfer equation is given by:

$$u\frac{\partial c}{\partial r} + \frac{v}{r}\frac{\partial c}{\partial \phi} + w\frac{\partial c}{\partial z} = \alpha_c \left[\frac{1}{r}\frac{\partial}{\partial r}\left(r\frac{\partial c}{\partial r} \right) + \frac{1}{r^2}\frac{\partial^2 c}{\partial \phi^2} + \frac{\partial^2 c}{\partial z^2} \right] \qquad (8)$$

Where α_c denote the solutal diffusion coefficient.

3.5 The Magnetohydrodynamics (MHD) Equations

In the presence of a magnetic induction, the motion of an electrically conducting fluid across magnetic lines of force generates a current. Fluid elements carrying currents, which traverse magnetic lines of force, give rise to an additional force acting on the elements Hurle (1994), which is called Lorentz force. The Lorentz force is defined as:

$$L = J \times B \qquad (9)$$

Where J is current density; according to the extended Ohm's law, it reads:

$$J = \sigma(E + \underline{V} \times B) \qquad (10)$$

Where σ is the electrical conductivity of the fluid (assumed isotropic) and $\underline{V}$ is the vector flow velocity. Equation (9) can be re-written as follows:

$$L = \sigma(E + \underline{V} \times B) \times B \qquad (11)$$

The components of the Lorentz force represent the components of the magnetic force in the Navier-Stokes equation, which was presented in Equations (1) to (3). In this study, the electric field, E, is neglected in equation (11). The electromagnetic stirring of the solution is achieved by a rotating magnetic field of intensity B and frequency ω placed around the heater ring. The applied rotating magnetic field can be described according to Ghaddar (1999) and Wang (2005) by:

$$\boldsymbol{B} = B\left[e_r \sin(\phi - \omega t) + e_\phi \cos(\phi - \omega t) \right] \qquad (12)$$

Where ω is the angular velocity of the magnet-driver, e_r and e_φ are the radial and angular unit vectors. To obtain an expression for the Lorentz force, the following assumptions are made, Ghaddar (1999) and Gelfgat and Priede (1995):

1. The azimuthal component of Lorentz force (F_φ^M) plays the dominant role.

2. The fluid motion is driven by the time average of the tangential component of the Lorentz force, namely.

3. The fluid rotation is considerable slower than the magnetic field frequency so it can be assumed that the radial and axial components of the Lorentz force are of the order $Ha/(Re_m)^{1/2} \leq 1$ and can be safely neglected.

4. The ampoule and the solid GeSi are assumed to be electrical insulators.

Therefore the Lorentz force will become;

$$F_\varphi^M = \frac{1}{2\pi} \int_0^{2\pi} \sigma\omega r B^2 \cos^2(\omega t - \varphi) d\omega t$$
$$= \frac{1}{2}\sigma\omega r B^2 \qquad (13)$$

3.6 Boundary Conditions

The boundary conditions used in the model are as follows:

a) At the solid/liquid interface and at the solid boundaries (ampoule lateral wall):

1) $u = 0, v = 0, w = 0$ (Non-slip condition)
2) $\frac{\partial c}{\partial r} = 0$

b) At the dissolution interface:

$c = c_1 = 0.15$

c) At the growth interface:

$c = c_2 = 0.02$

Where c_1 and c_2 are the concentration of the Silicon in the crystal growth process at dissolution and growth interface, respectively.

The value of the concentration of the growth interface is obtained from the Ge-Si phase diagram, Olesinski (1984)

4 Solution Technique

The non-dimensional governing equations along with the boundary conditions have been solved by the Galerkin finite element method. The CFD package, FIDAP, based on the finite element method, has been used in this study.

In the model, the solution is assumed to be incompressible viscous Newtonian fluid. Boussinesq approximation is introduced to account for density variations which bring buoyancy forces in the momentum equations. The simulation also incorporates the quasi-steady-state model of Ye (1996). This assumption is due to the slow growth rate for semiconductor materials, about 4 mm/day. The experimental temperature field is used to calculate the temperature field in the model.

4.1 Sensitivity Analysis

To get an optimum number of grids, mesh sensitivity analysis was examined for this study model. Performing a mesh sensitivity analysis is an integral part of producing accurate, time-efficient and cost-effective results. The source and the substrate zones have been kept at a constant mesh of 80 and 60 nodes respectively, in the axial direction. These zones are kept at constant axial mesh because they are solid and a finer mesh is not needed for improving numerical accuracy as the temperature gradient is relatively weak in those regions. The full Navier-Stokes equations, energy and mass transport equations have been solved in the solution zone only. The solvent (solution) was varied from 40 to 260 nodes in the axial direction in increments of 20. This was examined for two models, containing 40 and 60 circumferential nodes. The results show that there is a slight difference in the result between 40 and 60 nodes. The average Nusselt number across the solvent is used for mesh sensitivity because it is directly related to the driving force of the simulation. The average Nusselt number calculated for each case is listed in Table 1 which shows the average Nusselt number versus the axial number of nodes. It is clear that the optimum mesh is 60 by 240 nodes because the deviation of the Nusselt number starts to decrease at 220 axial nodes and almost no change is noticed at 240 and 260 axial nodes.

5 Results and discussion

In the last few years, much attention has been placed on examining the effects of rotating magnetic fields (RMF)

Table 1 : Mesh sensitivity analysis and comparison the average Nusselt number for 60 and 40 elements in circumferential direction

40 Circumferential Elements		60 Circumferential Elements	
Axial Elements	**Average Nusselt Number**	**Axial Elements**	**Average Nusselt Number**
40	1.653423	40	1.659502
60	1.597216	60	1.610607
80	1.560759	80	1.550888
100	1.537114	100	1.533077
140	1.512045	140	1.492088
160	1.492922	160	1.478915
180	1.472897	180	1.475208
200	1.463672	200	1.470661
220	1.454669	220	1.462937
240	1.446673	240	1.454958
260	1.445935	260	1.454123
280	1.444534	280	1.451857

Table 2 : Physical properties of GeSi used in the simulation, Saghir (1987)

Physical Properties of $Ge_{0.85}Si_{0.15}$		Physical Properties of $Ge_{0.98}Si_{0.02}$		Physical Properties of Ge	
Symbol	**Values**	**Symbol**	**Values**	**Symbol**	**Values**
c_p	$0.04008 J/g \cdot K$	c_p	$0.04008 J/g \cdot K$	c_p	$0.0390 J/g \cdot K$
T_m	$1100^o C$	T_m	$971^o C$	T_m	$935^o C$
α_c	$2.6 \times 10^{-4} cm^2/s$	α_c	$0.52 \times 10^{-4} cm^2/s$	α_c	$1.0 \times 10^{-4} cm^2/s$
α_T	$1.2 \times 10^{-1} cm^2/s$	σ	$2.5 \times 10^4 S/cm$	α_T	$1.2 \times 10^{-1} cm^2/s$
β_c	$0.005 1/at\%Si$	β_c	$0.0051/at\%Si$	β_c	$0.005 1/at\%Si$
β_T	$1.2 \times 10^{-4} 1/^o C$	β_T	$1.01 \times 10^{-4} 1/^o C$	β_T	$1.0 \times 10^{-4} 1/^o C$
κ	$0.2905 W/cm.K$	κ	$0.2559 W/cm.K$	κ	$0.25 W/cm.K$
μ	$7.4 \times 10^{-3} g/cm \cdot s$	μ	$8.3496 \times 10^{-3} g/cm \cdot s$	μ	$8.5 \times 10^{-3} g/cm \cdot s$
ν	$1.46 \times 10^{-3} cm^2/s$	ν	$1.53192 \times 10^{-3} cm^2/s$	ν	$1.5424 \times 10^{-3} cm^2/s$
ρ	$5.067 g/cm^3$	ρ	$5.4504 g/cm^3$	ρ	$5.51 g/cm^3$

on the growth of semiconductors materials that are derived from melts with liquid state electrical conductivity.

As explained before, application of a rotating magnetic field sets up a body force in the solution zone that tends to oppose the buoyancy-induced convection at the growth interface. In this study, the results for different rotational speeds (2, 7 and 10 rpm) of the magnetic field under uniform and non-uniform heater profile conditions are discussed for different levels of magnetic field intensities (B=2, 15 and 22 mT).

All the cases are related to terrestrial conditions.

The results are shown for the solvent region in a vertical plane, middle of solvent (z=2 cm) and near the growth interface (z=1.575 cm).

5.1 The Effect of Applied Rotating Magnetic Field under Uniform Heating Condition

Figures 4 to 6 show a vertical cut plane (frame (a)), horizontal cut plane near the growth interface (b) and silicon variation along the radial position in the middle of the solvent.

Figure 4 shows the results for the rotating magnetic field at 2 rpm with different magnetic field intensities (B=2, 15, 22 mT).
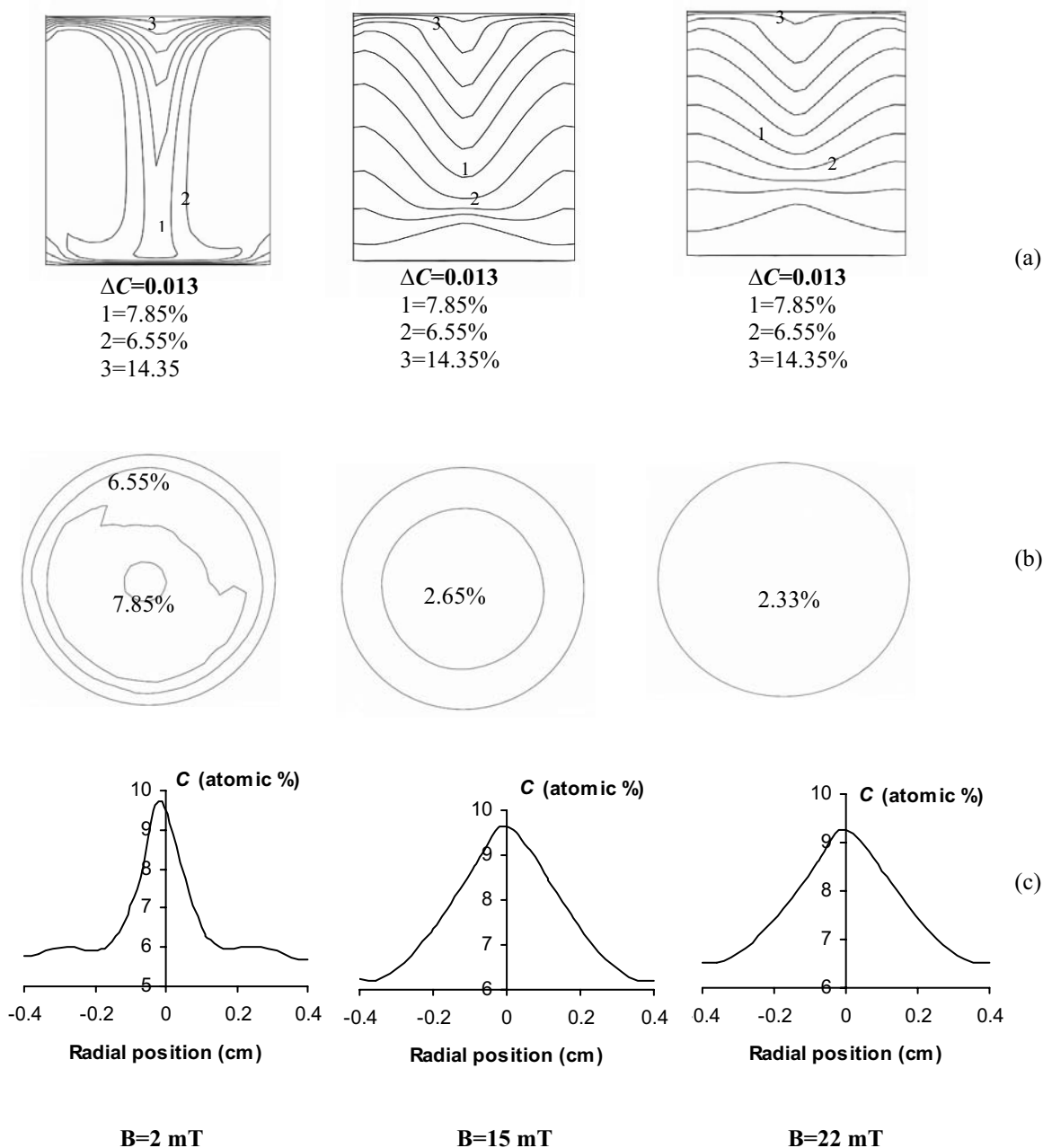
Figure 4 : Silicon contours in the solvent region for $\Omega = 2 \ rpm$ in the vertical plane (top), the horizontal plane near the growth interface at z =1.575 cm (middle) and the variation along radial direction in the middle of the solvent at z=2 cm (bottom), under uniform heating profile.

By examining the silicon distribution at the horizontal cut plane near the growth interface (0.075 cm above the growth interface), it is evident that when the magnetic field intensity is increased, the silicon contours tend to become more homocentric which is desirable for crystal growth (see Figure 4 frame b). Figure 4c shows the variation of the silicon concentration along the radial direc-

tion in middle of the solvent. It can be seen that there is a very large silicon concentration gradient for low magnetic field intensities; by increasing the magnetic field intensity, the silicon concentration behaviour become axisymmetric and more uniform.

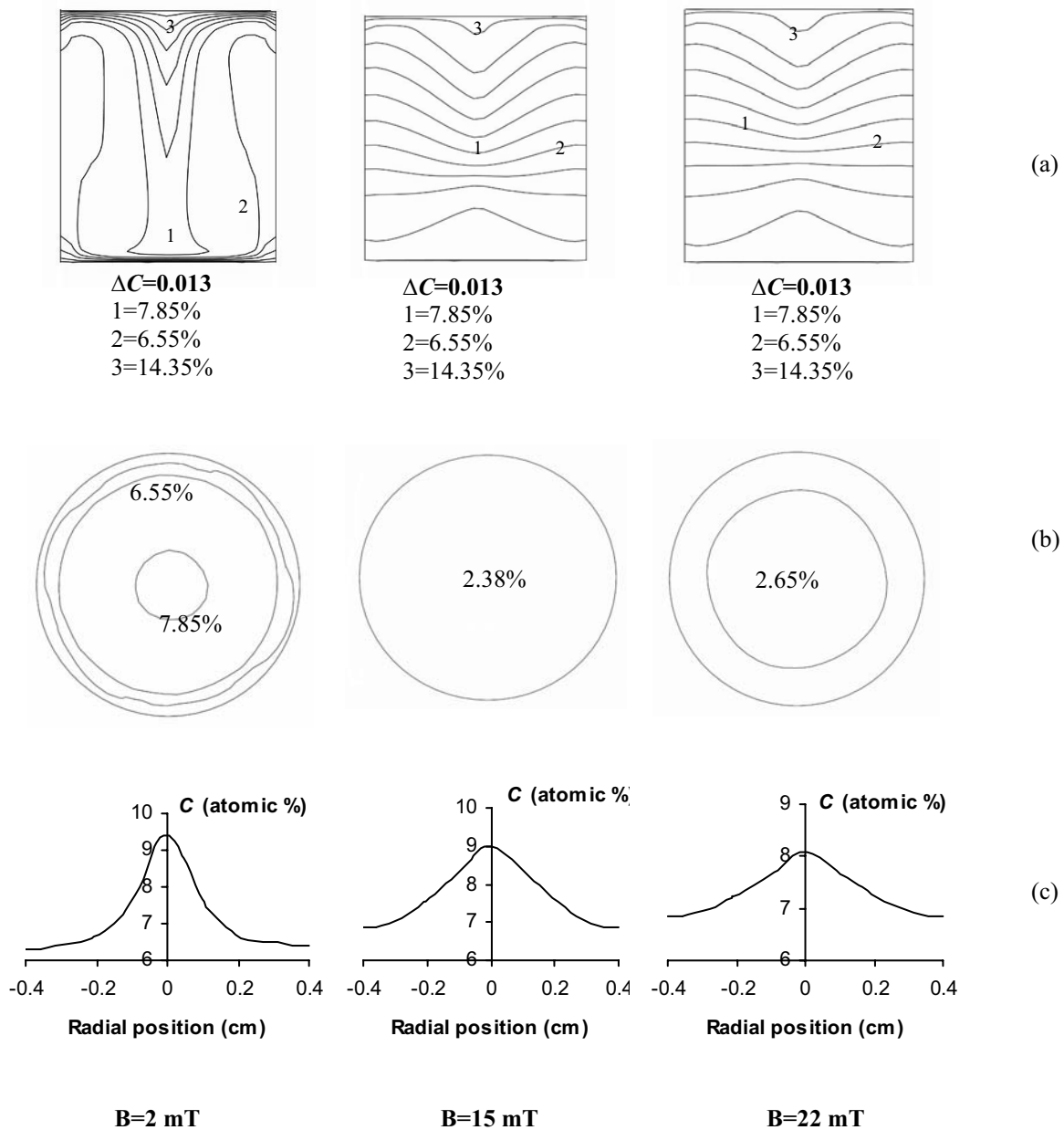The vertical cut planes (Figure 4a) show that the silicon contours become flatter and more uniform, particularly

Figure 5 : Silicon contours in the solvent region for $\Omega = 7\ rpm$ in the vertical plane (top), the horizontal plane near the growth interface at z =1.575 cm (middle) and the variation along radial direction in the middle of the solvent at z=2 cm (bottom), under uniform heating profile.

near the growth interface.

Figure 5 summarizes the silicon contours of rotational speed at 7 rpm for different magnetic field intensities (B=2, 15 and 22 mT). From the vertically cut planes, it can be seen that the silicon cells are more expanded and become flatter and linear when compared to a 2 rpm case (see Figure 5a). The horizontally cut planes near the growth interface show that the silicon contour cells

have become more homocentric than the 2 rpm case (see Figure 5b).

The silicon variation in the middle of the solvent (z=2 cm) along the radial position can be seen in Figure 5c. Unlike the 2 rpm case, for a low magnetic field intensity (B=2 mT), the silicon variation becomes symmetrical. Furthermore, the maximum silicon concentration becomes less comparing with the 2 rpm case. For exam-
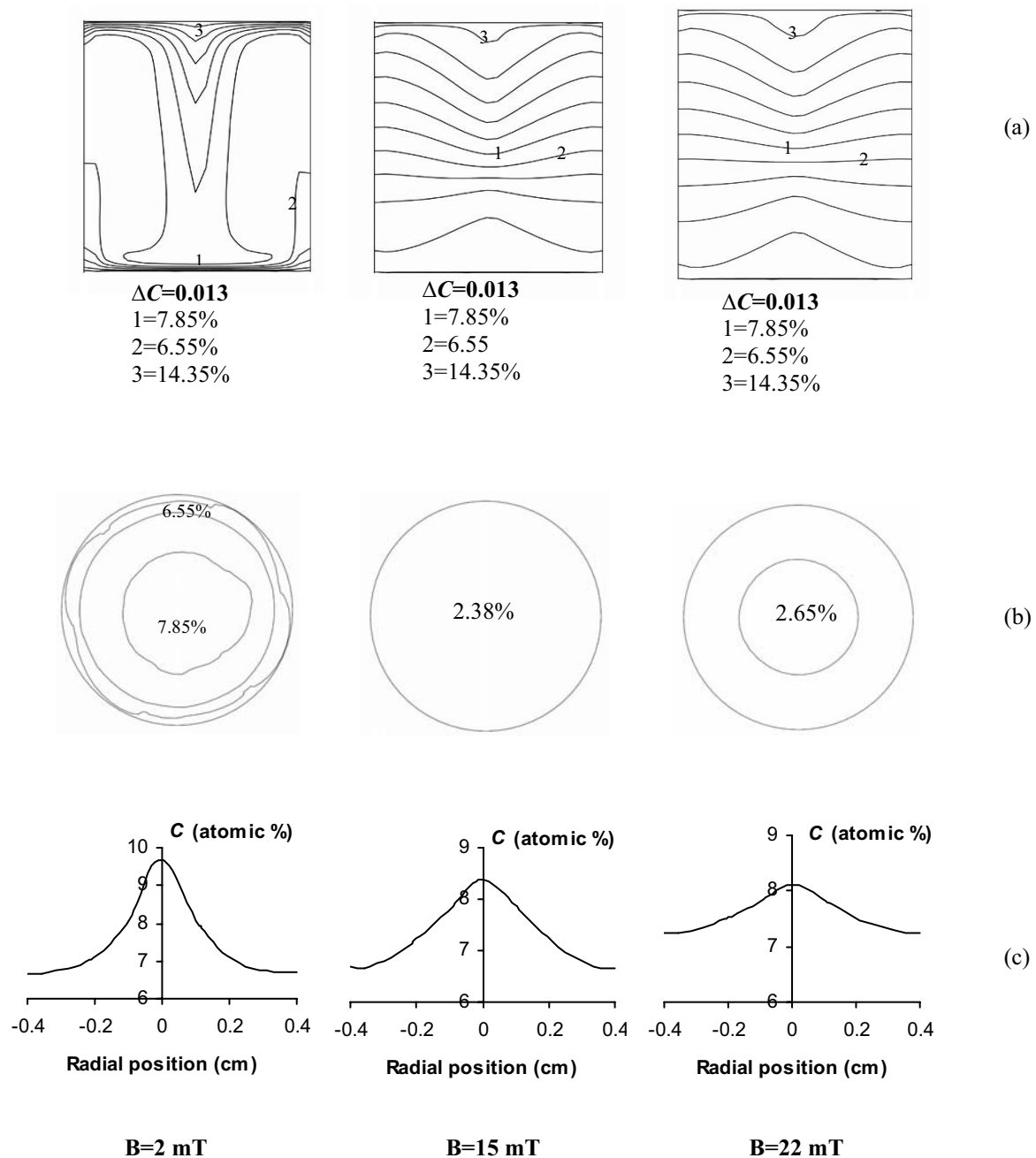
(a)

ΔC=**0.013**
1=7.85%
2=6.55%
3=14.35%

ΔC=**0.013**
1=7.85%
2=6.55
3=14.35%

ΔC=**0.013**
1=7.85%
2=6.55%
3=14.35%

6.55%

7.85%

2.38%

2.65%

(b)

C (atomic %)

Radial position (cm)

C (atomic %)

Radial position (cm)

C (atomic %)

Radial position (cm)

(c)

B=2 mT   **B=15 mT**   **B=22 mT**

Figure 6 : Silicon contours in the solvent region for $\Omega = 10$ *rpm* in the vertical plane (top), the horizontal plane near the growth interface at z =1.575 cm (middle) and the variation along radial direction in the middle of the solvent at z=2 cm (bottom), under uniform heating profile.

ple, it is equal to 9% at B=15 mT while it is equal to 9.6% in the 2 rpm case (see Figure 4c).

Figure 6 displays the results of the silicon contours at a rotational speed of 10 rpm for various levels of the magnetic field intensities (B=2, 15 and 22 mT). In this Figure, it can be noted that at a low magnetic field intensity

(B=2 mT) the silicon contours become less symmetric than those of the 7 rpm case at the same level of the magnetic field intensity (see Figure 5 and 6 frame b).

By applying a larger magnetic field intensity and a larger rotational mechanism (Figure 6c), it is found that the concentration gradient decreases and the difference between
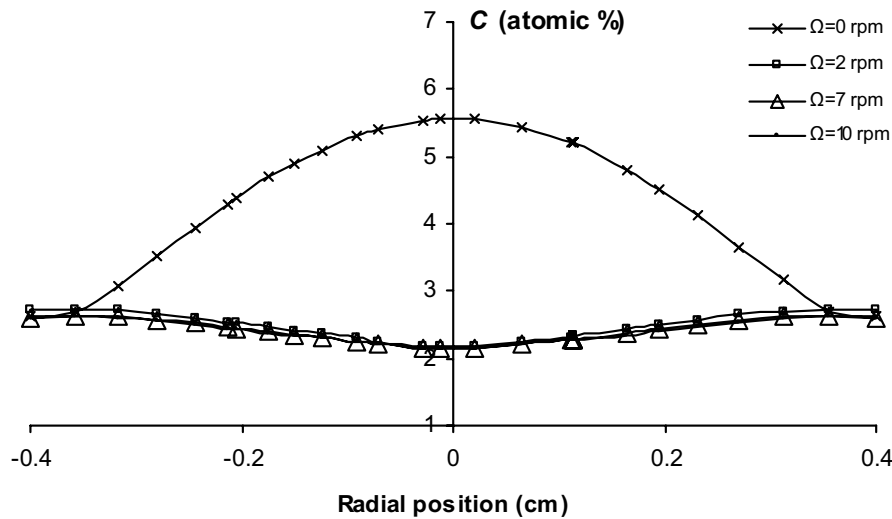
Figure 7 : Silicon distribution near the growth interface (z=1.575 cm) for different rotational speeds and B=15 mT under uniform heating profile.
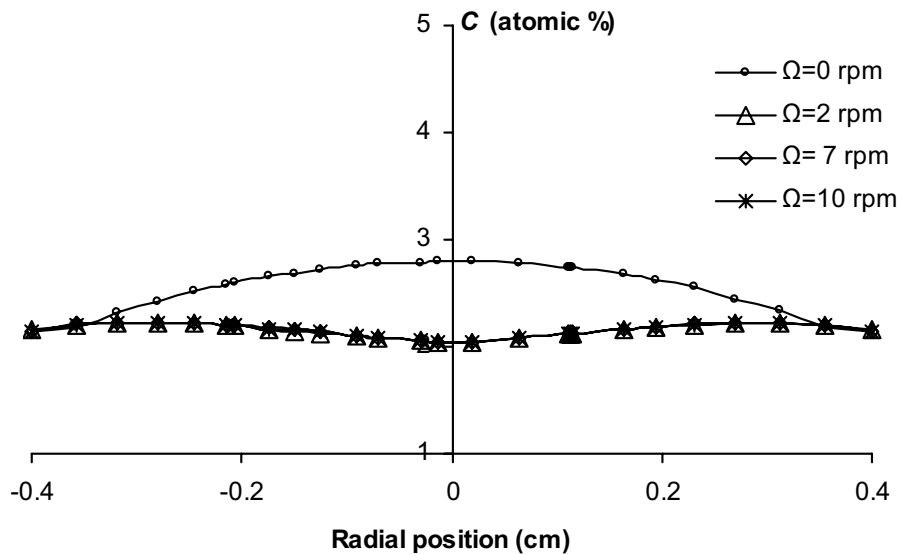

Figure 8 : Silicon distribution very close to growth interface (z=1.515 cm) for different rotational speeds and B=15 mT under uniform heating profile.

the maximum and the minimum concentration percentage drops. By comparing these results to the results of the axial magnetic field studied by Abidi (2005), it can be concluded that the RMF effect is better than that of an axial magnetic field.

Figure 7 shows the silicon variation along the radial direction for different rotational speeds at a magnetic field intensity of 15 mT. In this instance, it is quite clear that the rotational magnetic field (RMF) affects the silicon distribution near the growth interface. As a result, this distribution tends to become flatter and more uniform. In instances without a rotational magnetic field, the concentration shape appears convex. For crystal growth, it is desired to have a flat and a smooth concentration distribution along the growth interface. Thus, according to this Figure, the optimum crystal growth of GeSi occurs at a rotational magnetic field of 7 rpm and a magnetic field intensity of 15 mT.

The silicon variation located at 0.015 cm above the growth interface (very close to the growth interface) for different rotational speeds and B=15 mT is presented in Figure 8, Once again it can easily be seen that the silicon distribution tends to become flatter with the application of RMF.

5.2 The Effect of Applied Rotating Magnetic Field under Non-uniform Heating Condition

The non-uniform heater profile was investigated due to the fact that there is practically no heater profile which is uniform. Different magnetic field intensities (B=2 and 15 mT) for different rotational speeds (2 and 7 rpm) have been applied to the TSM model under a non-uniform heater profile condition.

Figures 9 and 10 show the results of the silicon concentration for low and high magnetic fields (B=2 and 15 mT) for the different rotational speeds 2 and 7 rpm, respectively. These Figures follow the same style of previous sections. From Figure 9, It can be seen that the silicon cells have disrupted and become asymmetrical at low magnetic field (B=2 mT). This behaviour is noticed in the vertical cut planes (see Figure 9a). The symmetry of silicon variation in the middle of the solvent along the radial direction under a uniform heater profile is destroyed when applying a non-uniform heater profile (see Figure 9c).

Figure 10 shows the silicon concentration for 7 rpm and different magnetic field intensities (B=2 and 15 mT). There is a significant change in the silicon contours at a low magnetic field (B=2 mT) which are disturbed and become unsymmetrical when compared with the uniform heating case. This change is noticed at the vertical cut plane. It can also be seen from the silicon variation along the radial position that becomes asymmetrical.

From the silicon contours at the RMF for 15 mT and 7 rpm, it is noticed that, there is no change in the vertical cut plane and horizontal cut plane near the growth interface when compared with the uniform case at the same RMF.

It is evident that the non-uniform heating profile has a significant effect when considering a low magnetic field intensity (as shown at B=2 mT for the speeds 2 and 7 rpm). As well, better results were found for the case with a rotational magnetic field of 7 rpm and 15 mT.

6 Conclusion

A three-dimensional model has been numerically simulated to illustrate the effects of applied rotating magnetic fields (RMF) on the flow during the crystal growth of $Ge_{0.98}Si_{0.02}$ by the traveling solvent method (TSM). It has been found that a RMF is a powerful tool for control of the compositional uniformity of the solution near the growth interface.

The results for uniform heating conditions have shown that the rotational magnetic field (RMF) affects the silicon distribution near the growth interface and this distribution becomes more flat and uniform; for a non-rotation condition, the concentration shape is convex. Optimum crystal growth of GeSi occurs at a rotational magnetic field of 7 rpm and a magnetic field intensity of 15 mT.

A non-uniform heating profile causes asymmetrical and disturbed silicon concentration. However, for the large magnetic field (15 mT), there is no significant change when applying the non-uniform heating profile with respect to the uniform case. A non-uniform heating profile has a significant effect on the low magnetic field intensity case (as shown at B=2 mT for the speeds 2 and 7 rpm).

Nomenclature

B magnetic field induction (Tesla)

B_o reference magnetic field induction (Tesla)

C solute concentration (atomic %)

c_o reference solute concentration (atomic %)

c_p specific heat at constant pressure (cal/g·K)

E electric field (volt/cm)

g gravity (cm/s^2)

g_o earth gravity (cm/s^2)

Ha Hartmann number: $Ha = |B_o|D\sqrt{\frac{\sigma}{\mu}}$

J current density (A/cm^2)

L Lorentz force (N)

P pressure (g/cm^2.s^2)

r radial direction (cm)

Re_m magnetic Reynolds number: $Re_m = \mu_o\sigma u_o D$

T temperature (^{o}C)

T_o reference temperature (^{o}C)

u radial velocity (cm/s)

$\underline{V}$ velocity vector (cm/s)

v circumferential velocity (cm/s)
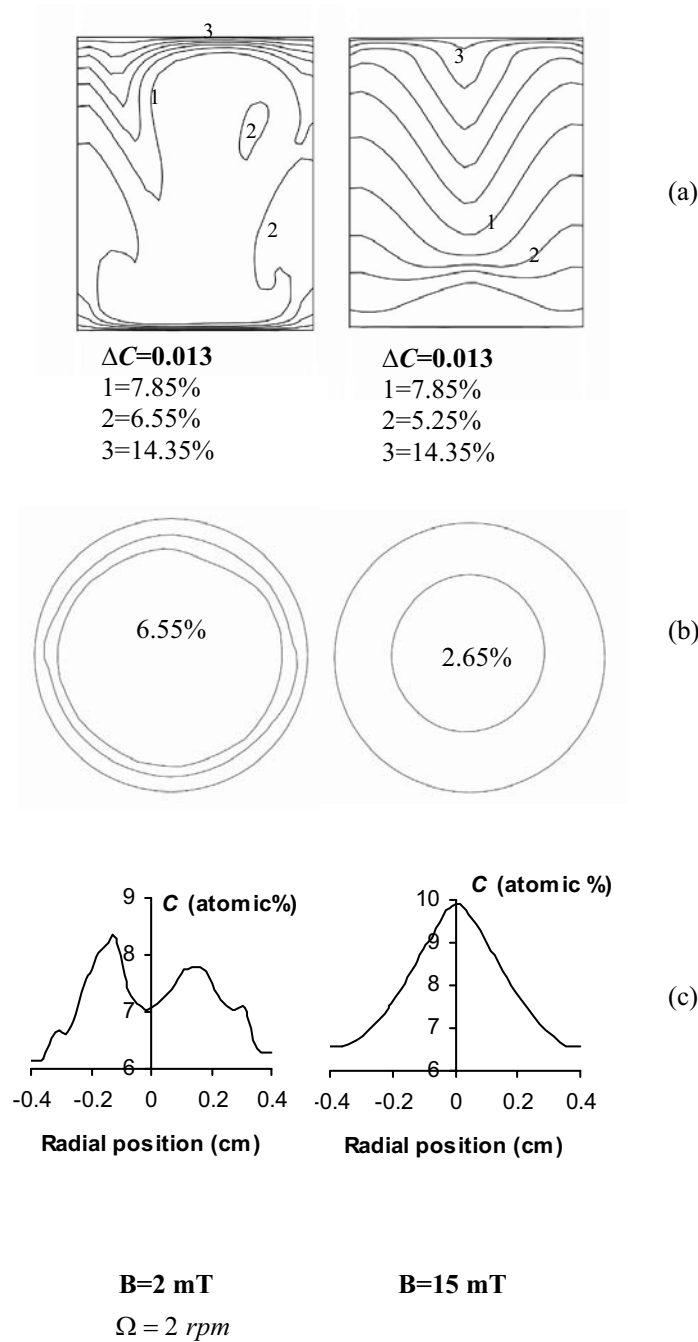
w axial velocity (cm/s)

z axial direction (cm)

Figure 9 : Silicon contours in the solvent region in the vertical plane (top), the horizontal plane near the growth interface at z =1.575 cm (middle) and the variation along radial direction in the middle of the solvent at z=2 cm (bottom), under non-uniform heating profile.

Greek Symbols

α_c solutal diffusivity of the species (cm^2/s)

β_c solutal expansion coefficient (1/at %Si))

β_T thermal expansion coefficient (1/^{o}C)

κ thermal conductivity (cal/s.cm.K)

μ dynamic viscosity (g/cm.s)

ν kinematic viscosity (cm^2/s)

ρ density (g/cm^3)

(a)

ΔC=0.013
1=7.85%
2=6.55%
3=14.35%

ΔC=0.013
1=7.85%
2=6.55%
3=14.35%

(b)

6.55%

2.38%

(c)

C (atom ic %')

C (atom ic %)

Radial position (cm)

Radial position (cm)
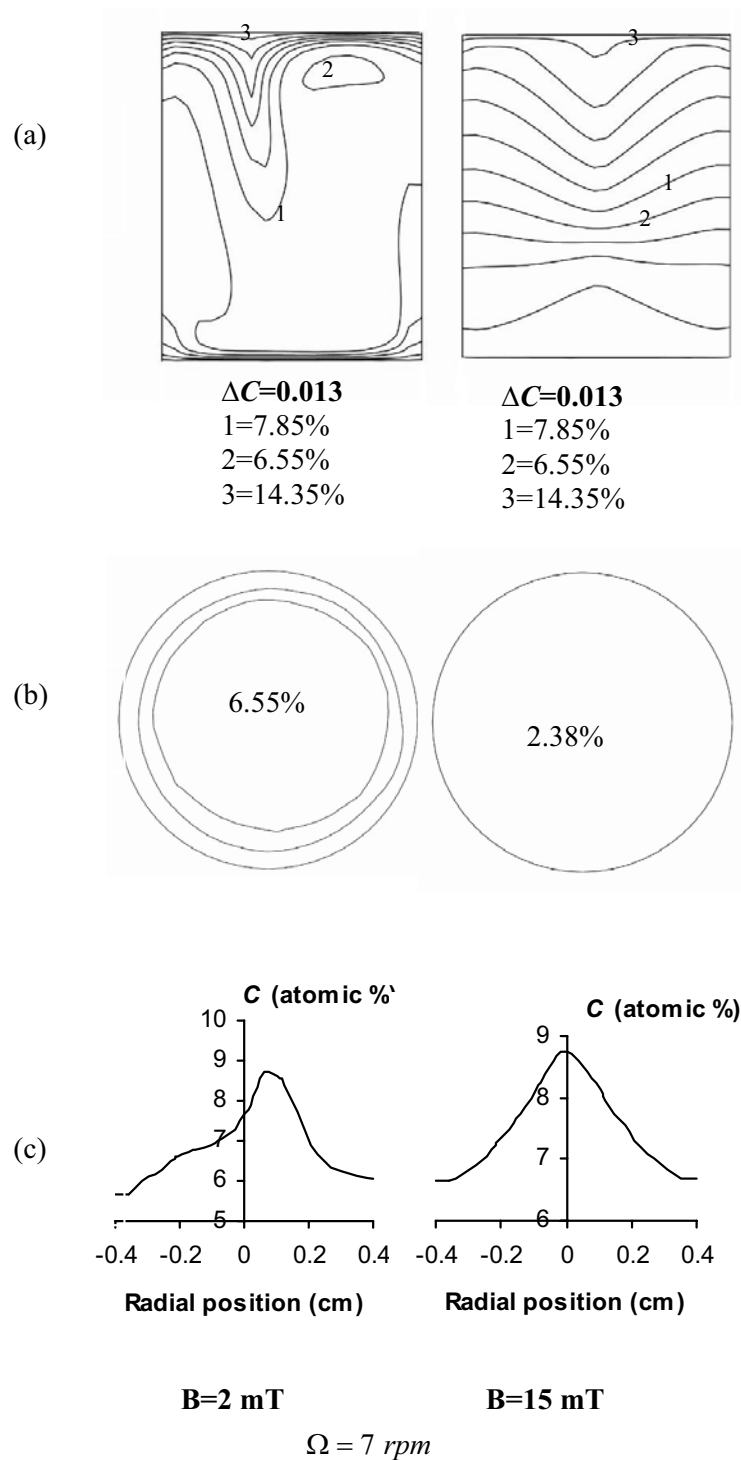
B=2 mT   **B=15 mT**

Ω = 7 *rpm*

Figure 10 : Silicon contours in the solvent region in the vertical plane (top), the horizontal plane near the growth interface at z =1.575 cm (middle) and the variation along radial direction in the middle of the solvent at z=2 cm (bottom), under non-uniform heating profile.

σ	electric conductivity (S/cm)	ω	angular velocity (rad/s)
φ	circumferential direction	Ω	rotational speed (rpm)

Subscripts

o   reference

References

Abidi, L; Saghir, M. Z.; Labrie, D. (2005): Use of an axial magnetic field to suppress convection in the solvent of $Ge_{0.98}Si_{0.02}$ grown by the traveling solvent method, *Int. J. Materials and Product Technology* vol. 22 pp. 2-19

Campbell, T. A.; Schweizer, M.; Dold, P.; Croll, A.; Benz, K. (2001): Float Zone Growth and Characterization of $Ge_{1-x}Si_x$ (x¡10%) Single Crystals, *Journal of Crystal Growth,* vol. 226 pp.231-239.

Gelfgat, Yu. M. and Priede, J., (1995): MHD Flows in a Rotating magnetic Field (a Review), *Magnetohydrodynamics*, vol. 31, Nos. 1-2, pp 188-200.

Gelfgat A. Yu., Rubinov A., Bar-Yoseph P.Z. and Solan A., (2005): On the Three-Dimensional Instability of Thermocapillary Convection in Arbitrarily Heated Floating Zones in Microgravity Environment , *FDMP: Fluid Dynamics and Materials Processing*, Vol. 1, No.1, pp 21-32

Ghaddar, C. K.; Lee, C. K.; Motakef S.; Gillies D. C. (1999): Numerical simulation of THM growth of CdTe in presence of rotating magnetic fields (RMF), *Journal of Crystal Growth* vol. 205 pp. 97-111.

Hurle, D.T.J. (1994): Handbook of Crystal Growth: Bulk Crystal Growth B: Growth mechanics and dynamic", North- Holland, Amsterdam.

Lan C. W., Yeh B.C., (2005): Effects of rotation on heat flow, segregation, and zone shape in a small-scale floating-zone silicon growth under axial and transversal magnetic fields, *FDMP: Fluid Dynamics and Materials Processing*, Vol. 1, No. 1, pp. 33-44.

Lappa M., (2005): Review: Possible strategies for the control and stabilization of Marangoni flow in laterally heated floating zones, *FDMP: Fluid Dynamics and Materials Processing*, Vol. 1, No.2, pp. 171-188.

Lent, B.; Dost, S.; Redden, R. F.; Liu, Y. (2002): Mathematical simulation of the traveling heater method growth of ternary semiconductor materials under suppressed gravity conditions, *Journal of Crystal Growth,* vol. 237–239 1876–1880

Liu, Y.; Dost, S.; Lent, B.; Redden, R. F. (2003): A Three Dimensional Numerical Simulation Model for the Growth of CdTe Single Crystals by Traveling Heater Method under Magnetic Field, *Journal of Crystal Growth*, vol. 254 pp. 285-297.

Liu, Y.C.; Okano, Y.; Dost, S. (2002), The Effect of Applied Magnetic Field on the Flow Structures in Liquid Phase Electroepitaxy-Three Dimensional Simulation Model, *Journal of Crystal Growth*, vol. 244 pp. 12-26.

Okano,Y; Nishino, S.; Ohkubo, S.; Dost, S. (2002): Numerical Study of Transport Phenomena in the THM growth of compound semiconductor crystal, *Journal of crystal growth,* vol. 237-239 pp. 1779-1784.

Olesinski, R. W.; Abbaschian, G. J. (1984): Bulletin of Alloy Phase Diagrams, 5 edition 180.

Ma N. and and Walker J. S. (2006): Electromagnetic Stirring in Crystal Growth Processes, *FDMP: Fluid Dynamics and Materials Processing*, Vol. 2, No. 2, pp. 119-126.

Saghir, M. Z. (1987): A Study of the Marangoni Convection on the Germanium Float Zone, *Low Gravity Science*, American Astronautical Society, vol. 67 pp. 77-100.

Salk, M; Fiederle M; Benz, K. W; Senchenkove, A. S; Egorov, A.V; Matioukhin, D. G. (1994): CdTe and $CdTe_{0.9}Se_{0.1}$ Crystals Grown by THM Using a Rotating Magnetic Field" *Journal of Crystal Growth*, vol. 138 pp. 161-167.

Senchenkov, A. S.; Barmin, I.V.; Tomson, A. S.; Krapukhin, V.V. (1999): Seedless THM growth of $Cd_xHg_{1-x}Te$ (x~0.2) single crystals within rotating magnetic field, *Journal of Crystal Growth,* vol. 197 pp552-556.

Sohail, M. and Saghir, M. Z. (2006): Three-Dimensional Modeling of the Effects of Misalignment on the Growth of Ge1-xSix by The Traveling Solvent Method, *FDMP: Fluid Dynamics and Materials Processing*, Vol. 2, No. 2, pp. 127-140.

Tsukada T., Kobayashi M., Jing C.J. and Imaishi N. (2005): Numerical simulation of CZ crystal growth of oxide, Fluid Dyn. Mater. Process, Vol. 1, No.1, pp. 45-

62.

Wang, X. D.; Li, T. J.; Fautrelle, Y.; Dupouy, M. D.; Jin J. Z. (2005): Two kinds of magnetic fields induced by one pair of rotating permanent magnets and their application in stirring and controlling molten metal flows" *Journal of the crystal growth* vol. 275 pp. 1473-1479.

Ye, X.; Tabarrok, B.; Walsh, D. (1996): The Influence of Thermosolutal Convection on CdTe growth by the Traveling Heater Method, *Journal of Crystal Growth*, vol. 169 pp. 525-530.

Yu, A.; Gelfgat, A.; Bar-Yoseph, P. Z.; Solan, A. (2001): Effect of axial magnetic field on three-dimensional instability of natural convection in a vertical Bridgman growth configuration, *Journal of Crystal Growth*, vol. 230, pp.63–69.